Vol. 93 (1997) ACTA PHYSICA POLONICA A No. 2

Proceedings of the 1st International Symposium on Scanning Probe Spectroscopy and Related Methods, Poznań 1997

A THEORETICAL ANALYSIS OF BALLISTIC ELECTRON EMISSION MICROSCOPY: BAND STRUCTURE EFFECTS AND ATTENUATION LENGTHS

P.L. DE ANDRES, K. REUTER*

Instituto de Ciencia de Materiales (CSIC), Cantoblanco, 28049 Madrid, Spain

F.J. GARCIA-VIDAL, F. FLORES

Dept. de Fisica Teorica de la Materia Condensada
Universidad Autonoma de Madrid, 28049 Madrid, Spain

U. HOHENESTER AND P. KOCEVAR

Institut für Theoretische Physik, Karl-Franzens-Universität, 8010 Graz, Austria

Using a quantum mechanical approach, we compute the ballistic electron emission microscopy current distribution in reciprocal space to compare experimental and theoretical spectroscopic $I(V)$ curves. In the elastic limit, this formalism is a "parameter-free" representation of the problem. At low voltages, low temperatures, and for thin metallic layers, the elastic approximation is enough to explain the experiments (ballistic conditions). At low temperatures, inelastic effects can be taken into account approximately by introducing an effective electron–electron lifetime as an imaginary part in the energy. Ensemble Monte Carlo calculations were also performed to obtain ballistic electron emission microscopy currents in good agreement with the previous approach.

PACS numbers: 61.16.Ch, 72.10.Bg, 73.20.At

1. Introduction

A very interesting application of the scanning tunneling microscope (STM) has become recently established as a technique on its own: the ballistic electron emission microscope (BEEM) [1]. In the standard version of this technique, the STM acts as a microscopy gun injecting a very narrow and coherent beam of electrons in a metallic layer deposited on a semiconductor. The injected electrons

*On leave from: Lehrstuhl für Festkörperphysik, University of Erlangen-Nürnberg, Germany.

propagate through the metallic layer and are finally detected in the semiconductor, after passing the metal–semiconductor interfacial Schottky barrier. Then, the standard model describes BEEM as a process consisting of three different steps [2]: tunneling of the electrons from the tip to the sample, propagation through the metallic layer and, finally, transmission across the metal–semiconductor interface.

In this paper, first of all, we concentrate our discussion in presenting a theoretical approach that describes the microscopic mechanism governing the propagation of the electrons from the tip to the metal–semiconductor interface. This approach takes into account the main effects associated with the electron band structure, and shows how coherent electron propagation through the metal layer results in the focussing of the electron beam and in a strong modification of the momentum electron distribution at the metal–semiconductor interface. Then, by calculating the transmission coefficient for this ideal interface we obtain the ideal BEEM current if no other scattering mechanism limits its intensity. In a final step we discuss some inelastic processes reducing the value of the total BEEM current. We analyse this problem in two different ways, by introducing an imaginary part in the frequency of the Green functions describing the propagation of electrons through the metal or by means of a k-space ensemble Monte Carlo technique. Both cases yield similar results and show how to analyze the electron–electron scattering process.

2. Theory for the electron propagation through the metal base

We discuss this propagation by introducing the following Hamiltonian:

$$\widehat{H} = \widehat{H}_{\mathrm{T}} + \widehat{H}_{\mathrm{S}} + \widehat{H}_{\mathrm{I}}, \tag{1}$$

where the tip $\widehat{H}_{\mathrm{T}}$, the metal $\widehat{H}_{\mathrm{S}}$, and the interaction $\widehat{H}_{\mathrm{I}}$ Hamiltonians are defined by the following equations [3]:

$$\widehat{H}_{\mathrm{T}} = \sum_{\alpha} \epsilon_{\alpha} \widehat{n}_{\alpha} + \sum_{\alpha,\beta} \widehat{T}_{\alpha\beta} \widehat{c}_{\alpha}^{\dagger} \widehat{c}_{\beta}, \quad \widehat{H}_{\mathrm{S}} = \sum_{i} \epsilon_{i} \widehat{n}_{i} + \sum_{i,j} \widehat{T}_{ij} \widehat{c}_{i}^{\dagger} \widehat{c}_{j} \qquad \text{and}$$

$$\widehat{H}_{\mathrm{I}} = \sum_{\alpha,j} \widehat{T}_{\alpha j} \widehat{c}_{\alpha}^{\dagger} \widehat{c}_{j}. \tag{2}$$

Here, α (greek subindexes) and i (latin subindexes) refer to the different tip and metal orbitals, while $\widehat{T}$ defines the hopping integrals between different orbitals. In our approach we assume Hamiltonians (2) to be well defined; in particular, the two first Hamiltonians yield the band structure and the electronic properties of the tip and the metal [4], respectively, and the third defines their coupling interaction.

We assume the tip and sample to have different Fermi levels, $E_{\mathrm{F}}(T)$ and $E_{\mathrm{F}}(M)$, with $E_{\mathrm{F}}(T) > E_{\mathrm{F}}(M)$ and $eV = E_{\mathrm{F}}(T) - E_{\mathrm{F}}(M)$. Then, we proceed to compute the tunneling currents and the induced metal density currents by using a Keldysh formalism [5]. The central objects in this formalism, the Green functions $\widehat{G}_{\alpha\beta}^{+-}$, $\widehat{G}_{ij}^{+-}$, or $\widehat{G}_{\alpha i}^{+-}$, are obtained from a Dyson-like equation through the Green functions of the uncoupled parts of the system, $\widehat{g}^{\mathrm{R}}$ and $\widehat{g}^{\mathrm{A}}$ (the retarded and advanced Green functions), and the different hopping elements, $\widehat{T}$ [6, 7]. From

$\widehat{G}^{+-}$, currents between sites a and b in the metal are obtained using the equation

$$J_{ab} = \int \mathrm{Tr}\{\widehat{T}_{ab}(\widehat{G}^{+-}_{ab} - \widehat{G}^{+-}_{ba})\}\mathrm{d}E, \tag{3}$$

where $\widehat{T}$ and $\widehat{G}$ are matrices associated with the orbitals located at sites a and b, and Tr means the trace of the matrix.

It has been shown elsewhere [6] that Eq. (3) leads to the following equation for the current between a and b:

$$J_{ab} = \frac{2e}{\pi\hbar}\mathcal{R}\int_{-\infty}^{\infty}\mathrm{d}E[f_{\mathrm{T}}(E) - f_{\mathrm{M}}(E)]\mathrm{Tr}\{\widehat{g}^{\mathrm{A}}_{1a}(E)\widehat{T}_{ab}\widehat{g}^{\mathrm{R}}_{b1}(E)\widehat{T}_{10}\widehat{\rho}_{00}(E)\widehat{T}_{01}\}, \tag{4}$$

where, for simplicity, we have assumed that a single active tip atom, 0, is only coupled to a single metal atom 1. Then, in Eq. (4), the term $\widehat{g}^{\mathrm{A}}_{1a}\widehat{T}_{ab}\widehat{g}^{\mathrm{R}}_{b1}$ plays the role, in our LCAO-formalism, of the term $\psi^*\nabla\psi$ defining the density current in elementary quantum theory. Moreover, the term $\widehat{T}_{10}\widehat{\rho}_{00}\widehat{T}_{01}$ is related to the tip–sample coupling and $[f_{\mathrm{T}}(E) - f_{\mathrm{M}}(E)]$ to the differences in the occupied states of the tip and sample (f is the corresponding Fermi distribution function).

Equation (4) is the basis for our calculation of the density currents inside the metal in real space. In these calculations, we obtain the retarded and advanced metal Green functions by means of a decimation technique [8], and use Eq. (4) to calculate J_{ab}.

The current distribution in reciprocal space is also necessary in order to match the metal wave functions with the semiconductor states at the metal–semiconductor interface. The $\boldsymbol{k}_{\|}$-space current ($\boldsymbol{k}_{\|}$ is the momentum parallel to the surface) between two layers, say p and q, $J_{pq}(\boldsymbol{k}_{\|})$, is given by an expression formally identical to Eq. (4). In particular, Fourier-transforming Eq. (4) we get the following equation:

$$J_{pq}(\boldsymbol{k}_{\|}) \equiv \int_{-\infty}^{\infty}\mathrm{d}E J_{pq}(\boldsymbol{k}_{\|}, E) = \frac{2e}{\pi\hbar}\mathcal{R}\int_{-\infty}^{\infty}\mathrm{d}E[f_{\mathrm{T}}(E) - f_{\mathrm{M}}(E)]$$

$$\times\mathrm{Tr}\{\widehat{g}^{\mathrm{A}}_{1p}(\boldsymbol{k}_{\|}, E)\widehat{T}_{pq}(\boldsymbol{k}_{\|})\widehat{g}^{\mathrm{R}}_{q1}(\boldsymbol{k}_{\|}, E)\widehat{T}_{10}\widehat{\rho}_{00}(E)\widehat{T}_{01}\}, \tag{5}$$

where $\widehat{T}_{10}\widehat{\rho}_{00}\widehat{T}_{01}$ is the same factor appearing in Eq. (4) that couples the tip (0) to the first layer (1) while $\widehat{g}^{\mathrm{A}}_{1p}(\boldsymbol{k}_{\|}, E)$ and $\widehat{g}^{\mathrm{R}}_{q1}(\boldsymbol{k}_{\|}, E)$ define the Green functions coupling layers $1 \rightarrow p$ and $q \rightarrow 1$, respectively.

From Eq. (5), using the advanced and retarded Green functions, we can easily calculate the $\boldsymbol{k}_{\|}$-space density currents inside the metal.

3. Real space and $\boldsymbol{k}_{\|}$-space current distributions

In this section, our formalism is applied to the case of the growth of an Au metal layer on a Si(111) orientation. The experimental evidence collected with LEED, Auger and STM for Au films on Si suggests that the metal grows in a (111)-crystalline direction, except for the first few layers near the interface that may present some disorder [9]. Accordingly, in our theoretical calculations we assume to have the tip located on top of a Au(111) surface, with the metal forming

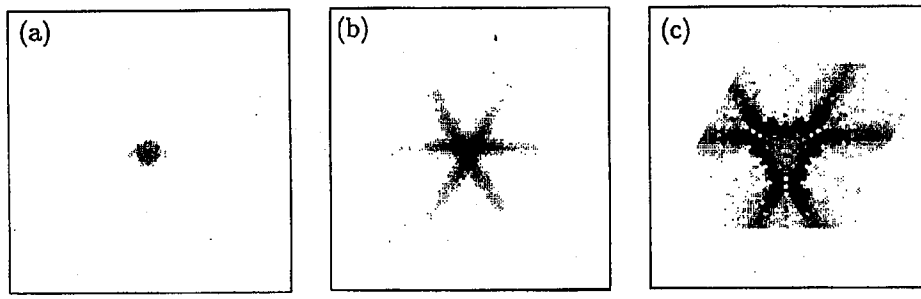

Fig. 1. Real space density current distributions calculated in the direction perpendicular to the layers (a) 2, (b) 5 and (c) 15 for a voltage of 1 eV.

a perfect structure extending up to the interface with the semiconductor. Injected metal density currents in real space or in $k_{\|}$-space are calculated using Eqs. (4) and (5). Regarding the real space distribution, in Fig. 1 we show our results for the density current calculated in the direction perpendicular to the layers $p = 2$, 5, and 15 for a voltage of 1 eV. These results show how the current injected in the metal evolves from a localised spot in the first layers to the formation of narrow beams and lines for deeper layers. This effect was predicted on the basis of a semiclassical approach [6] that yields the Green functions necessary to compute Eq. (4) and is now confirmed when working with more accurate, full quantum mechanical calculations.

We have also studied the $k_{\|}$-space current distribution. Although details will be published elsewhere, let us mention here our two main results: (a) first of all, we find our $k_{\|}$-distribution function independent from the layer we consider. This can be easily understood by realizing that once electrons are injected into the metal, and the coherent wave function is formed, their $k_{\|}$-momentum distribution cannot be changed unless other scattering mechanisms are present in the system. (b) On the other hand, for the propagation of electrons along the Au(111) direction, we find that electrons with small $k_{\|}$ component cannot propagate along the crystal: this is a consequence of having necks in the Au-Fermi surface along those 111-directions [10]. Our results also show that, outside these necks, electrons propagate with a practically constant distribution function in the solid angle of the momentum phase space. This angular distribution is one of the most important results found in our calculations as it is *essentially different from the conventional assumed forward cone* that people have used for the interpretation of BEEM results.

4. Ballistic currents. Transmission through the metal–semiconductor barrier

Previous calculations yield the propagation of the injected electrons across the metallic layer. In order to get the BEEM current, we have to match those metallic states to the semiconductor wave functions. In general, a full quantum mechanical calculation is complicated because both crystal surfaces, Au(111)

and Si(111), do not match. The simplest model, keeping the quantum character of the problem, for obtaining the transmission coefficient assumes the metal a free-electron gas, while the semiconductor is described using a reduced number of plane waves as discussed in [11]. From this approach we calculate the transmission coefficient, $T(\boldsymbol{k}_{\|}, E)$, and define the total BEEM current by the equation

$$I(V) = \int_{E_F+eV_0}^{E_F+eV} \mathrm{d}E \int_{1\mathrm{stB.Z.}} \mathrm{d}\boldsymbol{k}_{\|} J_{c-1,c}(\boldsymbol{k}_{\|}, E) \times T(\boldsymbol{k}_{\|}, E), \tag{6}$$

where c is the last metal layer, V_0 is the Schottky barrier ($eV - eV_0$ defines the window for the injected electrons contributing to the BEEM current), and the integral in the gold Brillouin zone only includes those $\boldsymbol{k}_{\|}$-points that can transmit electrons into the semiconductor — as measured by $T(\boldsymbol{k}_{\|}, E)$. This last integral is performed summing over a dense grid of special points [12].

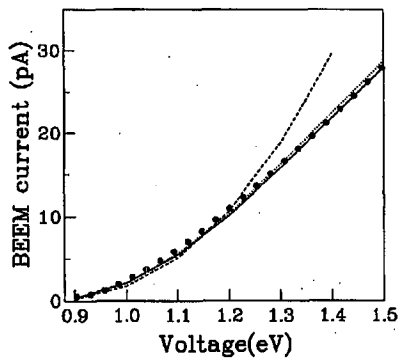

Fig. 2. Theoretical $I(V)$ curves for Au/Si(111), $d = 75$ Å (experimental values — solid circles — taken from Ref. [13]): ballistic current — dashed line, using a Green functions approach — continuous line, E-Monte Carlo technique — dotted line.

In Fig. 2 we show the ballistic current, calculated for a metal layer 75 Å thick, as a function of the applied voltage (V_0 is taken 0.9 eV). In the same figure we show the data collected by Bell at $T = 77$ K [13]. Comparing both curves we find an excellent agreement for $V < 1.2$ eV, and a small discrepancy between theory and experiment for larger voltages. Taking into account that our calculations are free of any adjustable parameter, we consider the agreement remarkable, although we stress this is mainly due to having a rather thin film. For thicker films, when electron scattering by phonons, electrons or impurities is important one needs to include those effects in the theory. We already see how these effects start to appear in thin films (see Fig. 2) for $V > 1.2$ eV. In particular, we argue that the small discrepancy found between theory and experiment in this particular case is basically due to the electron–electron scattering that reduces the ballistic current calculated previously assuming free propagation of the electrons in the metal layer. In this regards, notice that electron–phonon interaction cannot play an important role in the case we are analyzing, due to the low temperature, 77 K, of the experiments. At this temperature, the mean-free path for the electron–phonon

interaction is larger than 400 Å and its effect on the BEEM current for a metal layer thickness of 75 Å is negligible. We conclude that electron–electron interaction should be the main scattering process limiting the BEEM current for the high voltages of Fig. 2.

5. Electron–electron scattering

In the way we introduce this process, we keep in mind that this scattering process reduces, on the average, the energy of the incoming electrons by a half. For the voltages considered in Fig. 2, this implies that the electrons suffering an electron–electron scattering reduce their energy from the one necessary to contribute to the BEEM current. Accordingly, we can describe this process by means of an attenuation length that reduces exponentially the current injected in the metal. In accordance with a random phase approximation (RPA) calculation we take for this attenuation length the following functional form [14, 15]:

$$\lambda_{\mathrm{att}}(E) = \lambda^0 \frac{E/E_{\mathrm{F}}}{(E - E_{\mathrm{F}})^2}, \tag{7}$$

where λ^0 is taken 175 Å $(\mathrm{eV})^2$ to get the best fit to the experimental data. Given such an approximate mean free path, several reflections can add to the final BEEM current and we include them up to the third reflection on the surface.

Using Eq. (7) we have calculated the BEEM current in two ways:

(a) First, we introduce in the Green functions of Eq. (5) an imaginary part, η, in the energy E that we relate to λ_{att} by the equation

$$\eta = \frac{1}{\lambda_{\mathrm{att}}} \sqrt{\frac{2E}{m}}. \tag{8}$$

(b) We have also introduced an ensemble Monte-Carlo technique [16], whereby electrons, as injected in the metal by the tunneling process, are followed in their motion in real space and stopped after they have passed the interface or when they suffer an electron–electron scattering process. The relative fraction of electrons directly transmitted to the semiconductor determines the relative BEEM current as a function of the tunnel bias (details will be published elsewhere).

In Fig. 2 we show the theoretical BEEM current we have calculated using Eq. (7) and both, the Green functions approach and the E-Monte Carlo technique. The conclusions we draw from these results are the following: (a) Both theoretical techniques yield very similar results, confirming the validity of both approaches and the consistency of our calculations. (b) The agreement found between the theoretical and the experimental BEEM currents is excellent for all voltage biases. Although λ_{att} is taken to yield the best fit between theory and experiment, its value is not far from the one calculated from a first principles approach [14].

6. Conclusions

In conclusion we have presented a free parameter model for computing the ballistic current crossing the metal–semiconductor interface in a BEEM experiment. Our results present a good agreement with the data obtained for thin films, low temperature and low voltages. We believe that this shows the validity of our

model and confirms that the effect of the metal band structure is of paramount importance for obtaining the BEEM currents.

Moreover, we have also considered the effect of the electron–electron scattering on the final BEEM current and shown how a Green function approach or an E-Monte Carlo technique can be used for its evaluation. Our calculations for this case when an appropriate attenuation length for the electron–electron scattering is introduced, show an excellent agreement with the experimental evidence for the whole range of applied biases.

We acknowledge financial support from the Spanish CICYT under contracts number PBB94-53 and PB92-0168C. K.R. is grateful for financial support from SFB292 (Germany). We are grateful to Prof. K. Heinz for his support.

References

[1] W.J. Kaiser, L.D. Bell, *Phys. Rev. Lett.* **60,** 1406 (1988); L.D. Bell, W.J. Kaiser, *Phys. Rev. Lett.* **61,** 2368 (1988).

[2] For comprehensive reviews see M. Prietsch, *Phys. Rep.* **253,** 164 (1995), and L.D. Bell, W.J. Kaiser, *Ann. Rev. Mater. Sci.* **26,** 189 (1996).

[3] J.C. Slater, G.F. Koster, *Phys. Rev.* **94,** 1498 (1954).

[4] D.A. Papaconstantopoulos, *Handbook of the Band Structure of Elemental Solids*, Plenum, New York 1986.

[5] L.V. Keldysh, *Sov. Phys. JETP* **20,** 1018 (1965).

[6] F.J. Garcia-Vidal, P.L. de Andres, F. Flores, *Phys. Rev. Lett.* **76,** 807 (1996).

[7] P.L. de Andres, F.J. Garcia-Vidal, D. Sestovic, F. Flores, *Phys. Scr. Vol. T* **66,** 277 (1996).

[8] F. Guinea, C. Tejedor, F. Flores, E. Louis, *Phys. Rev. B* **28,** 4397 (1983).

[9] K. Oura, T. Hanawa, *Surf. Sci.* **82,** 202 (1979); A.K. Green, E. Bauer, *J. Appl. Phys.* **47,** 1284 (1976).

[10] D. Shoenberg, D.J. Roaf, *Philos. Trans. R. Soc.* **255,** 85 (1962); N.W. Ashcroft, N.D. Mermin, *Solid State Physics*, Holt-Saunders, Philadelphia 1981, Ch. 15.

[11] F. Garcia-Moliner, F. Flores, *Introduction to the Theory of Solid Surfaces*, Cambridge Univ. Press, Cambridge 1979.

[12] R. Ramirez, M.C. Böhm, *Int. J. Quantum Chem.* **30,** 391 (1986).

[13] L.D. Bell, *Phys. Rev. Lett.* **77,** 3893 (1996).

[14] C.R. Crowell, S.M. Sze, in: *Physics of Thin Films*, Vol. 4, Eds. G. Hass, R.F. Thun, Academic, New York 1976.

[15] A. Bauer, M.T. Cuberes, M. Prietsch, G. Kaindl, *Phys. Rev. Lett.* **71,** 149 (1993).

[16] U. Hohenester, P. Kocevar, P.L. de Andres, F. Flores, *Proc. 10th Conf. on Microscopy of Semiconducting Materials MSM-X, Oxford 1997*, Ed. T. Cullis, in press; U. Hohenester, P. Kocevar, P.L. de Andres, F. Flores, submitted to *Phys. Status Solidi B.*